Journal of Nuclear Medicine, published on March 20, 2020 as doi:10.2967/jnumed.119.239806

Title: ^{11}C-PABA as a Novel PET Radiotracer for Functional Renal Imaging: Preclinical and First-in-Human Studies

Authors: Camilo A. Ruiz-Bedoya[1,2,*], Alvaro A. Ordonez[1,2,*], Rudolf A. Werner[3], Donika Plyku[4], Mariah H. Klunk[1,2], Jeff Leal[4], Wojciech G. Lesniak[4], Daniel P. Holt[4], Robert F. Dannals[4], Takahiro Higuchi[5,6], Steven P. Rowe[4], Sanjay K. Jain[1,2,4]

Institutions:

[1] Center for Infection and Inflammation Imaging Research, Johns Hopkins University School of Medicine, Baltimore, MD, USA

[2] Department of Pediatrics, Johns Hopkins University School of Medicine, Baltimore, MD, USA

[3] Department of Nuclear Medicine, Hannover Medical School, Hannover, Germany

[4] Russell H. Morgan Department of Radiology and Radiological Sciences, Johns Hopkins University School of Medicine, Baltimore, MD, USA

[5] Okayama University Graduate School of Medicine, Dentistry and Pharmaceutical Sciences, Okayama, Japan

[6] Department of Nuclear Medicine, University Hospital, University of Würzburg, Würzburg, Germany

*Co-first authors

Running title: ^{11}C-PABA PET renal imaging

Address for correspondence:

Sanjay K. Jain, M.D

Department of Pediatrics, Johns Hopkins University School of Medicine

1550 Orleans Street

CRB-II Room 1.09

Baltimore, MD, USA

Email: sjain5@jhmi.edu

Phone: 410-502-8241

Co-first authors:

Camilo A. Ruiz-Bedoya, MD

Post-doctoral Fellow

Department of Pediatrics, Johns Hopkins University School of Medicine

1550 Orleans Street

CRB-II Room 237

Baltimore, MD, USA

Email: cruizbe1@jhmi.edu

Phone: 410-614-3051

Alvaro A. Ordonez, MD

Department of Pediatrics, Johns Hopkins University School of Medicine

1550 Orleans Street

CRB-II Room 3M.54

Baltimore, MD, USA

Email: aordone2@jhmi.edu

Phone: 410-614-4218

Word count: 4689

Funding: This work was funded by the National Institutes of Health (Director's Transformative Research Award R01-EB020539, R01-HL131829, and R01-EB025985) to S.K.J., and the Department of Defense's Congressionally Directed Medical Research Programs PR-171338P1 to S.K.J. R.A.W. was funded by the German Research Foundation (DFG), through the Clinician-Scientist Program PRACTIS.

ABSTRACT

para-Aminobenzoic acid (PABA) has been previously used as an exogenous marker to verify completion of 24-hour urine sampling. Therefore, we hypothesized that radiolabeled PABA with ^{11}C could allow high-quality dynamic PET of the kidneys while reducing the radiation exposure due to its short biological and physical half-lives. We evaluated if ^{11}C-PABA could visualize renal anatomy and quantify function in healthy rats, rabbits, and first-in-human studies in healthy volunteers. **Methods:** Healthy rats and rabbits were injected with ^{11}C-PABA intravenously. Subsequently, a dynamic PET was performed followed by post-mortem tissue biodistribution studies. ^{11}C-PABA PET was directly compared with the current standard, ^{99m}Tc-MAG3 in rats. Three healthy human subjects also underwent dynamic PET after intravenous injection of ^{11}C-PABA. **Results:** In healthy rats and rabbits, dynamic PET demonstrated a rapid accumulation of ^{11}C-PABA in the renal cortex, followed by rapid excretion through the pelvicalyceal system**.** In humans, ^{11}C-PABA PET was safe and well tolerated. There were no adverse or clinically detectable pharmacologic effects in any subject. The cortex was delineated on PET, and the activity gradually transited to the medulla and then renal pelvis with high spatiotemporal resolution. **Conclusion:** ^{11}C-PABA demonstrated fast renal excretion with very low background signal in animals and humans. These results suggest that ^{11}C-PABA could be used as a novel radiotracer for functional renal imaging, providing high-quality spatiotemporal images with low radiation exposure.

Keywords: PABA; renal imaging; PET; renography; translational science.

INTRODUCTION

The use of molecular imaging to evaluate renal function has been an evolving field for many decades (*1*). Based on radiolabeled agents with high renal clearance, initial approaches were focused on technetium-99m radiopharmaceuticals [e.g., ^{99m}Tc-mercaptoacetyltriglycin (^{99m}Tc-MAG3)] and planar gamma cameras. While these techniques are still widely used in clinical practice, they have some major limitations including two-dimensional information with a concomitant lack of accurate anatomic correlation, low spatial resolution, and low signal/background ratios. The soft-tissue attenuation may also reduce diagnostic accuracy and limit reliable quantification (*2*). Implementation of single-photon emission computed tomography (SPECT) for renal imaging led to improvements in image contrast and spatial resolution. However, in recent years there has been a shift towards the development of positron emission tomography (PET) renal imaging agents. PET offers multiple advantages such as three-dimensional dynamic visualization of the kidneys without organ overlap, higher sensitivity and signal/background ratio, and absolute camera-based quantification with higher counts. Consequently, PET requires administration of much lower doses of radioactivity and provides higher accuracy measurements of regional radiopharmaceutical tissue concentrations (*2-4*). Novel agents for PET renal imaging that have been evaluated with promising results include ethylenediaminetetraacetic acid labeled with gallium-68 (^{68}Ga-EDTA), fluorodeoxysorbitol with fluorine-18 (^{18}F-FDS), non-peptide angiotensin 1 (AT_1) antagonist with carbon-11 (^{11}C-L-159884), ^{11}C-acetate, *para*-^{18}F-aminohippurate (^{18}F-PFH), and the tubular function reflecting radiotracer $Re(CO)_3$-N-([^{18}F]fluoroethyl)iminodiacetic acid ($Re(CO)_3$[^{18}F]FEDA) (*2-8*).

para-Aminobenzoic acid (PABA) is a non-toxic B-complex vitamin with fast renal excretion that has been used since the 1980s as an exogenous marker to verify the completion of

24-hour urine sampling (*9,10*). While PABA undergoes hepatic metabolism by phase II conjugation via N-acetyltransferase 1 and glycine conjugation, all its metabolites are renally excreted (*11,12*). By targeting the incorporation of PABA into the folate synthesis of bacteria, with low uptake in mammalian tissues and rapid renal elimination, radiolabeled analogs of PABA are being developed for bacteria-specific imaging (*13-15*). We hypothesized that the high renal concentration, excretion, and performance of ^{11}C-PABA, as well as the potential for low radiation exposure, could be valuable characteristics for a renal imaging agent. In this study, we describe ^{11}C-PABA PET renal imaging in two healthy animal species and first-in-human studies in healthy volunteers.

MATERIALS AND METHODS

All animal protocols were approved by the Johns Hopkins University Biosafety, Radiation Safety, and Animal Care and Use Committees. Human studies were approved by the Johns Hopkins Institutional Review Board and carried out under the auspices of the Radioactive Drug Research Committee program.

Synthesis of ^{11}C-PABA

^{11}C-PABA was synthesized as a sterile, pyrogen-free solution with high radiochemical purity and specific activity (163.7 ± 40.9 GBq/μmol) under current good manufacturing practices (cGMP) conditions at the Johns Hopkins Hospital PET center (*16*).

Animal Studies

Healthy Wistar rats (Charles River Laboratories, Wilmington, MA, USA) weighing 301.5 ± 33.2 g (three females, one male) were injected with 22.3 ± 3.9 MBq of ^{11}C-PABA through a

tail-vein catheter, and dynamic PET was performed immediately thereafter using a nanoScan PET/CT (Mediso USA, Boston, MA, USA) with 15 one-minute and 6 five-minute frames for a total acquisition of 45 minutes. Healthy New Zealand White rabbits (Charles River Laboratories) weighing 3.0 ± 0.2 kg (two females) were intravenously injected with 51.9 ± 3.9 MBq of ^{11}C-PABA, followed by a 40-minute dynamic PET using the nanoScan PET/CT. The acquisition parameters were 15 one-minute and 5 six-minute frames for a total acquisition time of 40 minutes. A CT was also acquired for anatomic co-registration for all animals. Quantitative analysis was performed by placing seven volumes of interest using the CT as a reference within the kidneys: outer layer (corresponding to renal cortex), inner layer (corresponding to renal pelvis), intermediate layer (corresponding to renal medulla), and the bladder (only in rats). Renal perfusion was observed by visual assessment of ^{11}C-PABA transit through the abdominal aorta after the injection. The images were analyzed using VivoQuant 4.0 (Invicro, Boston, MA, USA) and visualized using Amide 1.0.4. Maximal parenchymal uptake activity is represented as T_{max}, which is the time from injection to peak activity on the renogram. The half-life is represented as $T_{1/2}$, which is the time from T_{max} to a 50% decrease. Relative renal uptake of the right and left kidney is expressed as the percentage of the total uptake.

Postmortem Tissue Biodistribution

Four additional healthy female Wistar rats (235.1 ± 28.9 g of weight) were simultaneously injected intravenously with 26.5 ± 1.5 MBq of ^{11}C-PABA and 18.1 ± 0.6 MBq of ^{99m}Tc-MAG3 (Cardinal Health, Dublin, OH, USA). The animals were sacrificed 30 minutes post-injection, and the tissues were harvested to quantify the associated radioactivity using an automated γ-counter [1282 Compugamma Gamma Counter CS, LKB Wallac (Mt. Waverley, Victoria, Australia)]. The measurements for ^{99m}Tc-MAG3 were performed two hours after those

for ^{11}C-PABA. The tissue biodistribution data are presented as percent injected dose per gram of tissue (%ID/g).

Dosimetry

Four healthy mice (CBA/j, Jackson Laboratory, Bar Harbor, ME, USA) were injected with 47.73 ± 2.59 MBq of ^{11}C-PABA through a tail-vein catheter, and dynamic PET was performed immediately thereafter over 85 minutes as described above. Volumes of interest were drawn on the CT images of a selection of mouse organs: brain, heart, lungs, liver, muscle, large intestine, kidneys, bladder, and bone marrow to obtain the activity concentration. These values were used to calculate human organ absorbed doses and time-integrated activity coefficients using the MIRD S value methodology as implemented in the OLINDA/EXM software package (*17-20*). Detailed methods for this analysis are provided in the Supplemental data.

First-in-Human Studies

Three healthy volunteers (2 male and 1 female) ≥18 years old were recruited from an ongoing first-in-human ^{11}C-PABA PET study at the Johns Hopkins Hospital (Table 1). The Johns Hopkins Institutional Review Board approved this study and all subjects signed a written informed consent. Pre-study evaluation included a medical history, a physical examination with vital signs, and laboratory tests (comprehensive metabolic panel to include alkaline phosphatase, total bilirubin, liver transaminase levels and renal function - blood urea nitrogen, creatinine). The eligibility criteria included laboratory evaluation within 28 days before enrollment showing normal liver function. Female subjects were screened for pregnancy and excluded if pregnant or lactating. Other exclusion criteria included subjects with hypertension, diabetes mellitus, body mass index <18.5 or >30 kg/m^2, family history of renal disease or a urinary tract infection in the prior 6 months. Subjects who had been treated with an investigational drug, investigational

biologic, or investigational therapeutic device within 30 days before radiotracer administration were also excluded. After written informed consent was obtained, subjects were injected with ^{11}C-PABA followed by a 30-minute dynamic single-bed PET scan using a Biograph mCT 128-slice PET/CT (Siemens Healthineers, Erlangen, Germany) operating in 3D emission mode. The subjects were positioned supine with the arms raised above their head, and a scout scan encompassing the abdomen was used to locate the kidneys for the PET acquisition. The acquisition area included both kidneys in a one-bed position. A 30-minute list-mode acquisition was started just before radiotracer injection. The reconstructed images consist of 10 frames for five seconds, 20 frames for fifteen seconds, and 25 frames for sixty seconds. A low-dose CT was subsequently acquired for anatomic localization and attenuation correction. Subjects were asked to empty their bladder prior to injection and after the imaging was completed. To perform the quantitative analysis, seven volumes of interest were manually drawn using the CT as a reference as described for the preclinical experiments, plus the abdominal aorta. The bladder was excluded from the acquisition field. Renal perfusion was determined by visual assessment of the ^{11}C-PABA transit through the abdominal aorta after the injection. The images were analyzed with Mirada XD (Mirada Medical, Oxford, United Kingdom) and PMOD (PMOD Technologies, Zurich, Switzerland) for dynamic quantification. Amide 1.0.4 and Imager-4D (*21*) were used for data visualization. A post-study follow-up was performed at 25 days after imaging over the telephone to assess for any side effects or other issues.

Statistical Analysis

For the animal imaging studies, data are represented on a linear scale as the average of the percentage injected dose per cubic centimeter (%ID/cc) ± standard deviation (SD). Data for post-mortem biodistribution is represented as percent injected dose per gram of tissue (%ID/g).

For human imaging studies, data are represented on a linear scale as average standardized uptake value (SUV) ± SD. All statistical analyses were performed using Prism 8 (GraphPad Software, San Diego, CA, USA).

RESULTS

Renal Kinetics of ^{11}C-PABA in Healthy Rats and Rabbits

Whole-body dynamic PET revealed rapid concentration of ^{11}C-PABA in the kidneys and its elimination through the bladder in rats. Minimal signal was observed from other organs. Visual assessment of the renal perfusion showed vascular blood flow, followed by a gradual accumulation of the radiotracer in the renal cortex with the subsequent transition of the activity into the collecting system (Figs. 1A and 1B). The time-activity curve renogram demonstrated a T_{max} of 8.5 ± 3.9 minutes in both kidneys, followed by a rapid transit into the pelvicalyceal system, with a $T_{1/2}$ of 32.2 ± 13.1 minutes. The differential renal uptake was 49 ± 3.1% and 50.9 ± 3.1% for the right and left kidneys, respectively. As would be predicted, the excretion phase correlated with increased uptake in the bladder (Fig. 1C). Post-mortem tissue biodistribution of ^{11}C-PABA and ^{99m}Tc-MAG3 was directly compared by measuring organ-associated radioactivity 30 minutes after simultaneous injection of both radiotracers in the same animals (Fig. 2). A lower tissue background was evident with ^{11}C-PABA compared to that of ^{99m}Tc-MAG3.

In healthy rabbits, ^{11}C-PABA PET also demonstrated high radiotracer excretion through the kidneys with a low background from other organs. Visual assessment of the renal perfusion showed the accumulation of the radiotracer in the renal cortex after 3 minutes post-injection, with a later transition into the renal pelvicalyceal system (Figs. 3A and 3B). Time-activity curves

demonstrated a T_{max} of 8.2 ± 1.3, a $T_{1/2}$ of 36.5 ± 11.6 minutes, and a relative renal uptake of 50.7 ± 1.8% and 49.3 ± 1.8% for the right and left kidneys, respectively (Fig. 3C).

Dosimetry

The calculated time-integrated activity coefficients (TIAC) are shown in Supplemental Table 1. The longest TIACs were observed in the bladder wall and contents. The urinary bladder, followed by the kidneys and lungs, received the highest absorbed dose (Supplemental Fig. 1 and Supplemental Table 2). The absorbed dose for the urinary bladder wall was 0.05 ± 0.01 mGy/MBq. The effective dose was estimated to be 0.0039 ± 0.0006 mSv/MBq.

Spatiotemporal Resolution and Renal Kinetics of ^{11}C-PABA in Healthy Volunteers

Two male and one female, healthy adult volunteers with an age range of 23-30 years were enrolled. The mean administered activity and mass were 680.1 ± 7.8 MBq (range, 671.2-685.6 MBq) and 593.3 ± 142.9 ng (range, 470-750 ng), respectively. There were no adverse or clinically detectable pharmacologic effects in any subject. All patients had a normal glomerular filtration rate (GFR) (Table 1). No renal anatomical abnormalities were found in any subject. In a dynamic PET acquisition centered on the kidneys, ^{11}C-PABA rapidly localized to the kidneys with minimal signal in other surrounding structures in the same field (Supplemental Video, available at: http://jnm.snmjournals.org). The abdominal aorta and renal arteries were detected after twenty seconds post-injection, with a T_{max} of 24.1 ± 7.6 seconds (Fig. 4A). The activity gradually accumulated in the renal cortex, reaching a maximal parenchymal uptake at 3.0 ± 0.4 minutes (Fig. 4B). The T_{max} on the right and left renal pelvis was 9.4 ± 5.4 minutes (Supplemental Fig. 2). The $T_{1/2}$ on the renal cortex was 23.3 ± 7.5 minutes and the average right and left renal cortical uptake for all time-points was 50.9 ± 4.3% and 49.06 ± 4.3%, respectively.

DISCUSSION

The use of PET for renal imaging is an emerging field with several advantages to evaluate structural abnormalities and quantification of kidney function. Compared to single-photon imaging, PET offers several key advantages for renal radionuclide imaging (*2,6*). These include, but are not limited to, better spatiotemporal resolution and absolute camera-based quantification (*4*). In addition, time-of-flight technology and improved reconstruction algorithms may allow for further decreasing the necessary amount of injected radioactivity. Moreover, PET allows for a precise elimination of background activity from surrounding organs (e.g. from the major vessels), and threshold-based approaches can be used to define the activity in the cortex and renal collecting system. Conversely, for renal scintigraphy, volumes of interest normally cover the entire kidneys to generate a renogram (*4*). Taken together, these advantages of PET radiopharmaceuticals for renal functional assessment could account for a clinical benefit. For instance, common gamma-emitting agents may underestimate the relative functional performance of one of the kidneys; one example would be the malrotation of a single kidney, which can have an impact on donating a kidney for transplantation (*22*). Other clinical applications may also include monitoring of therapy-induced renal remodeling, e.g. after abdominal radiation therapy (*23*). Renal parenchymal loss can be either diffuse or focal and occurs at even low doses such as 10 Gy. Volumes of interest derived by PET studies that cover "areas at risk" in the renal cortex or medulla may allow monitoring of renal injury after radiation or may even have predictive potential prior to therapy. Given these benefits, several PET radiotracers have been evaluated for renal imaging with promising results (*2,7*). With the benefits of a longer radiological half-life, ^{18}F-FDS has also been recently evaluated as a potential renal imaging agent (as a replacement for ^{99m}Tc-DTPA) in healthy and diseased rats as well as

healthy human subjects (*24-26*). Compared to ^{99m}Tc-DTPA, the tubular function reflecting radiotracer ^{99m}Tc-MAG3 has a more efficient extraction fraction (twice that of ^{99m}Tc-DTPA), which renders it as the preferred imaging agent in patients with suspected obstruction and impaired renal function (*27*). Not surprisingly, ^{99m}Tc-MAG3 is the radiotracer of choice in clinical routine and used in approximately 70% of the scans in the United States (*27*). However, recent years have witnessed an expanded use of PET given its advantages over SPECT (*28,29*). Thus, PET agents with the potential to replace ^{99m}Tc-MAG3 are needed.

The exclusive renal excretion of PABA has been previously used to assess 24-hour urine tests. While PABA is metabolized by the liver, all its metabolites are also renally excreted (*9,10*). In fact, one of its main metabolites, *para*-aminohippuric acid, has been used as a gold standard to measure effective renal plasma flow due to its high renal tubular secretion, as well as active glomerular filtration once it enters into the kidneys (*30*). Radiolabeling PABA with ^{11}C provides high-quality dynamic images of the kidneys while reducing the radiation exposure due to the short biological and radiological half-life of PABA and ^{11}C, respectively, enabling its use in young children. ^{11}C-PABA PET renal imaging in two different mammalian models (rats and rabbits) showed rapid localization of the radiotracer in the kidneys with low background signal from other organs. Murine data-based human dosimetry analysis of ^{11}C-PABA showed an effective dose 1.6 times lower than that of ^{99m}Tc-MAG3 (*1*). Based on these results, we performed first-in-human ^{11}C-PABA PET studies in three healthy subjects. The near-perfect split renal function observed in the small animal models and human subjects without known underlying renal disease suggests the potential of ^{11}C-PABA to detect unilateral renal disease and/or obstruction.

While the clinical implementation of ^{11}C-PABA would be limited to locations with an on-site cyclotron, the intrinsic low radiation exposure of ^{11}C-PABA is particularly well-suited to pediatric populations. However, further preclinical and clinical studies are required to understand the potential use of this radiotracer in specific conditions. The present feasibility study has limitations. Patients were not encouraged to drink water prior to the PET scan and a specific amount of water was not administered during the study. Further, although the first-in-human results are encouraging, a larger number of patients is needed to confirm these preliminary findings.

CONCLUSION

We describe a novel ^{11}C-based tracer used for PET renal functional imaging. In healthy rats, rabbits, and humans, ^{11}C-PABA demonstrated rapid renal excretion with a very low background signal. These results suggest that ^{11}C-PABA could be used as a novel imaging radiotracer to evaluate renal kinetics and anatomy, providing high-quality images of the kidneys with low radiation exposure compared to the standard of care (SPECT and planar imaging).

ACKNOWLEDGMENTS

We thank the patients who participated in the study. Additionally, we want to thank Allen Chen, Rehab Abdallah, and Corina Voicu (Johns Hopkins Hospitals) for coordinating the human imaging studies, and their assistance with image protocol and acquisition.

Disclosures: A.A.O. and S.K.J. are co-inventors on a pending patent application US2019050529 covering ^{11}C-PABA for renal imaging filed by Johns Hopkins University.

Authors contributions: C.A.R-B., A.A.O. and S.K.J. conceptualized and designed the study. C.A.R-B., A.A.O. and M.H.K. performed animal experiments. D.P.H. and R.F.D. synthesized ^{11}C-PABA. D.P. performed the dosimetry analysis. A.A.O., S.P.R., and S.K.J. recruited and consented healthy volunteers. C.A.R-B., A.A.O., R.A.W., and J.L. analyzed the imaging data. W.G.L. and T.H. aided with imaging and data analysis. C.A.R-B., A.A.O. and S.K.J. wrote the initial draft and all co-authors participated in editing the final manuscript. S.K.J. provided funding and supervised the project.

Conflict of interest: No potential conflicts of interest relevant to this article exist

KEY POINTS

Question: What is the value of using ^{11}C-PABA for PET renal imaging?

Pertinent findings: In healthy rats and rabbits, dynamic PET demonstrated a rapid accumulation of ^{11}C-PABA in the renal cortex, followed by rapid excretion through the pelvicalyceal system**.** In humans, ^{11}C-PABA PET was safe and well tolerated. The cortex was delineated on PET, and the activity gradually transited to the medulla and then renal pelvis with high spatiotemporal resolution.

Implications for patient care: These findings argue in favor of using ^{11}C-PABA as a novel imaging radiotracer to evaluate renal kinetics and anatomy, providing high-quality images of the kidneys with low radiation exposure compared to the standard of care (SPECT and planar imaging).

REFERENCES

1. Blaufox MD, De Palma D, Taylor A, et al. The SNMMI and EANM practice guideline for renal scintigraphy in adults. *Eur J Nucl Med Mol Imaging.* 2018;45:2218-2228.

2. Werner RA, Chen X, Lapa C, et al. The next era of renal radionuclide imaging: novel PET radiotracers. *Eur J Nucl Med Mol Imaging.* 2019;46:1773-1786.

3. Pathuri G, Sahoo K, Awasthi V, Gali H. Renogram comparison of p-[^{18}F] fluorohippurate with o-[^{125}I] iodohippurate and [^{99m}Tc] MAG3 in normal rats. *Nucl Med Commun.* 2011;32:908-912.

4. Hofman MS, Hicks RJ. Gallium-68 EDTA PET/CT for renal imaging. *Semin Nucl Med.* 2016;46:448-461.

5. Lipowska M, Jarkas N, Voll RJ, et al. $Re(CO)_3$([^{18}F] FEDA), a novel ^{18}F PET renal tracer: Radiosynthesis and preclinical evaluation. *Nucl Med Biol.* 2018;58:42-50.

6. Szabo Z, Xia J, Mathews WB, Brown PR. Future direction of renal positron emission tomography. *Semin Nucl Med.* 2006;34:36-50.

7. Szabo Z, Alachkar N, Xia J, Mathews WB, Rabb H. Molecular imaging of the kidneys. *Semin Nucl Med.* 2011;41:20-28.

8. Normand G, Lemoine S, Le Bars D, et al. PET [^{11}C] acetate is also a perfusion tracer for kidney evaluation purposes. *Nucl Med Biol.* 2019;76-77:10-14.

9. Bingham S, Cummings JH. The use of 4-aminobenzoic acid as a marker to validate the completeness of 24 h urine collections in man. *Clin Sci (Lond)*. 1983;64:629-635.

10. Jakobsen J, Pedersen AN, Ovesen L. Para-aminobenzoic acid (PABA) used as a marker for completeness of 24 hour urine: effects of age and dosage scheduling. *Eur J Clin Nutr*. 2003;57:138-142.

11. Lebel S, Nakamachi Y, Hemming A, Verjee Z, Phillips MJ, Furuya KN. Glycine conjugation of para-aminobenzoic acid (PABA): a pilot study of a novel prognostic test in acute liver failure in children. *J Pediatr Gastroenterol Nutr*. 2003;36:62-71.

12. Tabor CW, Freeman MV, Baily J, Smith PK. Studies on the metabolism of para-aminobenzoic acid. *J Pharmacol Exp Ther*. 1951;102:98-102.

13. Ordonez AA, Weinstein EA, Bambarger LE, et al. A systematic approach for developing bacteria-specific imaging tracers. *J Nucl Med.* Jan 2017;58:144-150.

14. Mutch CA, Ordonez AA, Qin H, et al. [^{11}C] Para-aminobenzoic acid: a positron emission tomography tracer targeting bacteria-specific metabolism. *ACS Infect Dis*. 2018;4:1067-1072.

15. Zhang Z, Ordonez AA, Wang H, et al. Positron emission tomography imaging with 2-[^{18}F]F-p-aminobenzoic acid detects *Staphylococcus aureus* infections and monitors drug response. *ACS Infect Dis.* 2018;4:1635-1644.

16. Holt DP, Kalinda AS, Bambarger LE, Jain SK, Dannals RF. Radiosynthesis and validation of [Carboxy-^{11}C]4-aminobenzoic acid ([^{11}C]PABA), a PET radiotracer for imaging bacterial infections. *J Labelled Comp Radiopharm.* 2019;62:28-33.

17. Stabin MG, Sparks RB, Crowe E. OLINDA/EXM: the second-generation personal computer software for internal dose assessment in nuclear medicine. *J Nucl Med.* 2005;46:1023-1027.

18. Bolch WE, Eckerman KF, Sgouros G, Thomas SR. MIRD pamphlet no. 21: a generalized schema for radiopharmaceutical dosimetry—standardization of nomenclature. *J Nucl Med.* 2009;50:477-484.

19. Keenan MA, Stabin MG, Segars WP, Fernald MJ. RADAR realistic animal model series for dose assessment. *J Nucl Med.* 2010;51:471-476.

20. Valentin J. Basic anatomical and physiological data for use in radiological protection: reference values: ICRP Publication 89. *Ann ICRP.* 2002;32:1-277.

21. Rowe SP, Solnes LB, Yin Y, et al. Imager-4D: New software for viewing dynamic pet scans and extracting radiomic parameters from PET data. *J Digit Imaging.* 2019;32:1071-1080.

22. Weinberger S, Baeder M, Scheurig-Muenkler C, et al. Optimizing scintigraphic evaluation of split renal function in living kidney donors using the geometric mean method: a preliminary retrospective study. *J Nephrol.* 2016;29:435-441.

23. Maturen KE, Feng MU, Wasnik AP, et al. Imaging effects of radiation therapy in the abdomen and pelvis: evaluating "innocent bystander" tissues. *Radiographics.* 2013;33:599-619.

24. Wakabayashi H, Werner RA, Hayakawa N, et al. Initial preclinical evaluation of ^{18}F-fluorodeoxysorbitol PET as a novel functional renal imaging agent. *J Nucl Med.* 2016;57:1625-1628.

25. Werner RA, Wakabayashi H, Chen X, et al. Functional renal imaging with 2-deoxy-2-^{18}F-fluorosorbitol PET in rat models of renal disorders. *J Nucl Med.* 2018;59:828-832.

26. Werner RA, Ordonez AA, Sanchez-Bautista J, et al. Novel functional renal PET imaging with ^{18}F-FDS in human subjects. *Clin Nucl Med.* 2019;44:410-411.

27. Taylor AT. Radionuclides in nephrourology, part 1: Radiopharmaceuticals, quality control, and quantitative indices. *J Nucl Med.* 2014;55:608-615.

28. Rowe SP, Gorin MA, Pomper MG. Imaging of prostate-specific membrane antigen using [^{18}F]DCFPyL. *PET Clin.* 2017;12:289-296.

29. Werner RA, Chen X, Rowe SP, Lapa C, Javadi MS, Higuchi T. Moving into the next era of PET myocardial perfusion imaging: introduction of novel ^{18}F-labeled tracers. *Int J Cardiovasc Imaging.* 2019;35:569-577.

30. Juillard L, Janier MF, Fouque D, et al. Dynamic renal blood flow measurement by positron emission tomography in patients with CRF. *Am J Kidney Dis.* 2002;40:947-954.

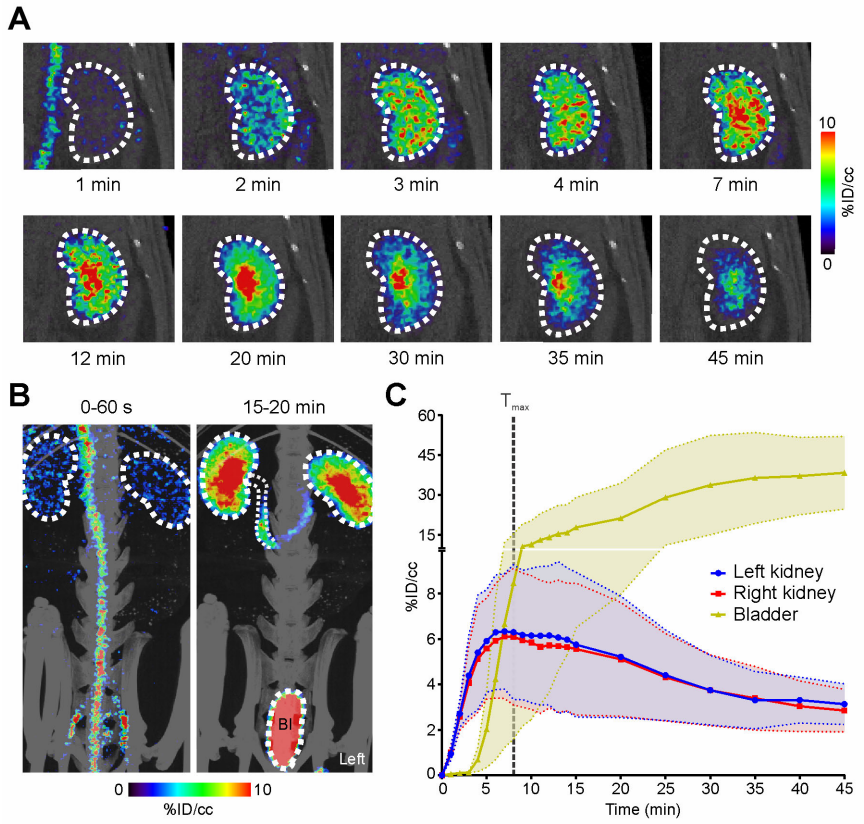

Figure 1. ^{11}C-PABA PET/CT renal imaging in healthy rats. (A) Coronal dynamic ^{11}C-PABA PET of the right kidney from a representative rat shows rapid cortical uptake after 2 minutes, followed by rapid clearance through the pelvicalyceal system. (B) The maximum intensity projections of a representative rat injected with ^{11}C-PABA showed the abdominal aorta and iliac arteries 60 seconds post-injection, as well as high activity in the bladder after 20 minutes, with low background signal in other tissues. Bl = bladder. (C) Average ^{11}C-PABA time-activity curves (renogram) of the kidneys and bladder. Data presented as mean (solid lines) and standard deviation (shaded areas), n=4.

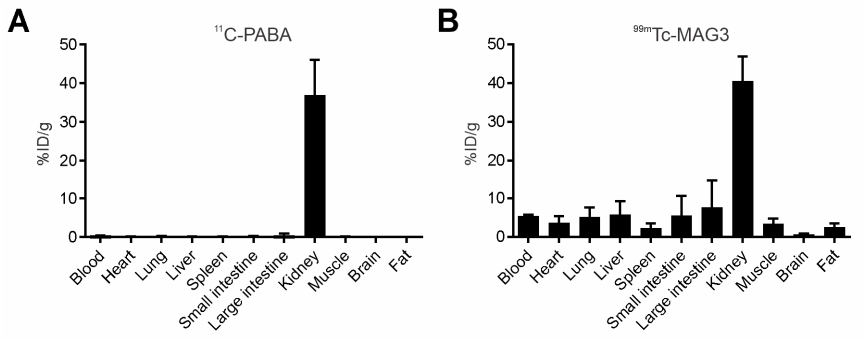

Figure 2. ^{11}C-PABA and ^{99m}Tc-MAG3 tissue biodistribution in rats. Healthy rats were injected intravenously simultaneously with ^{11}C-PABA and ^{99m}Tc-MAG3 and sacrificed 30 minutes after injection. ^{99m}Tc-MAG3 counts were performed two hours after those for ^{11}C-PABA, when the signal from ^{11}C (physical half-life of 20 min) would have completely decayed. (A) The tissue biodistribution of ^{11}C-PABA was primarily within the kidneys with very low activity in all the other measured organs. (B) Conversely, the biodistribution of ^{99m}Tc-MAG3 had higher background activity. Data presented as mean and standard deviation, n=4.

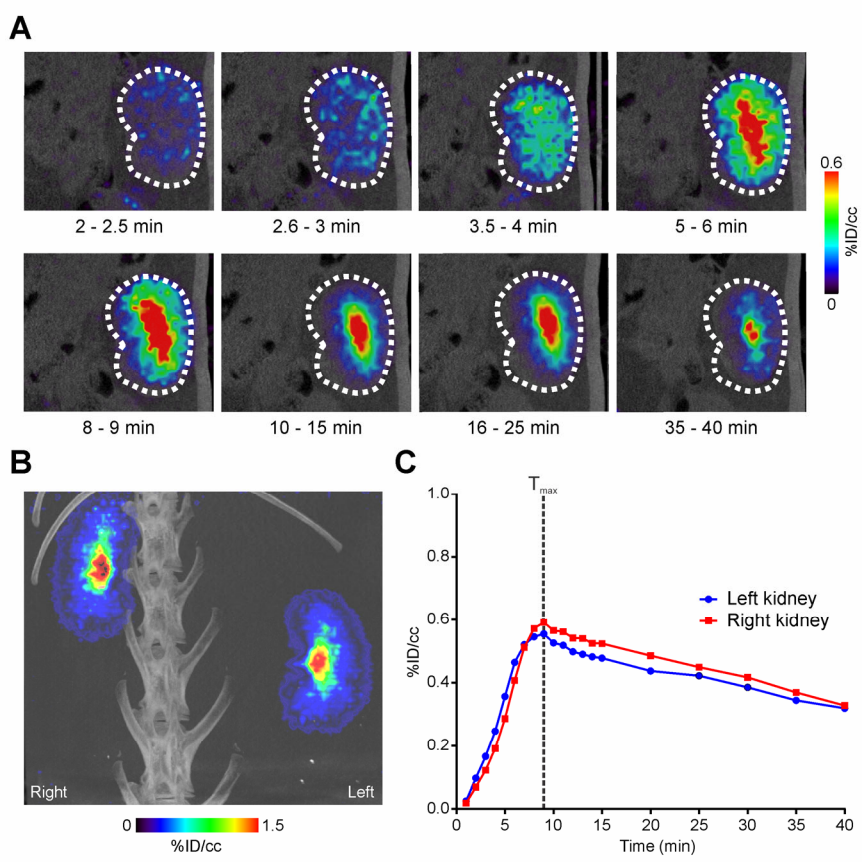

Figure 3. ^{11}C-PABA PET/CT renal imaging in healthy rabbits. (A) Coronal ^{11}C-PABA PET/CT sections of the right kidney of a representative rabbit. After injection, ^{11}C-PABA rapidly delineates the renal cortex, followed by accumulation in the pelvicalyceal system. (B) The maximum intensity projection of ^{11}C-PABA PET/CT at 20 minutes showed similar uptake in the left and right kidneys, with low background from other organs. (C) Time-activity curves (renogram) of ^{11}C-PABA were calculated and averaged for the left and right kidney. Data is represented as mean, n=2.

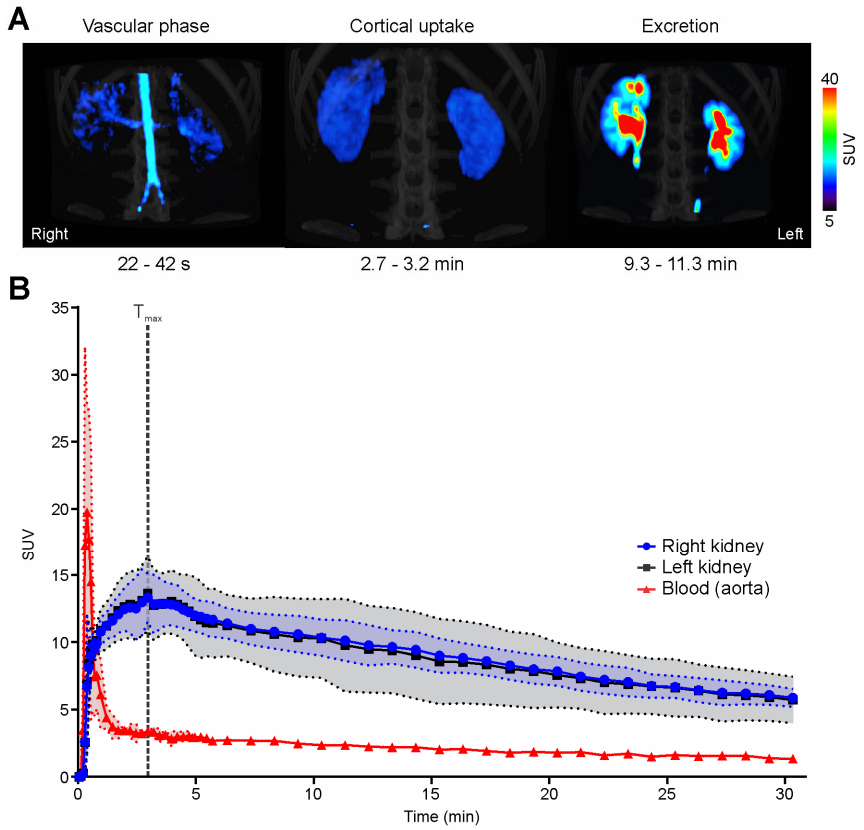

Figure 4. ^{11}C-PABA PET renal imaging in healthy human subjects. (A) Maximum intensity projections of the ^{11}C-PABA PET/CT of a representative subject. The vascular phase is observed after 22 seconds post-injection demonstrating renal perfusion. The cortical uptake phase was evident within 2.7 and 3.2 minutes, with maximal parenchymal uptake in the renal cortex. The excretory phase was seen after 9 minutes indicating the maximal uptake in the pelvicalyceal system. (B) Time-activity curve (renogram) of ^{11}C-PABA for the renal cortex and blood (aorta). Data represented as mean (solid lines) and standard deviation (shaded areas), n=3.

Table 1. Characteristics of human subjects. Body mass index (BMI), glomerular filtration rate (GFR).

Participant ID	**Gender**	**Age** (years)	**BMI** (kg/m^2)	**Creatinine** (mg/dL)	**GFR** ($mL/min/1.73m^2$)	**Albumin** (g/dL)	**^{11}C-PABA injected dose** (MBq)
1	M	23	21	0.8	154	4.9	685.6
2	M	25	20	0.8	143	4.8	671.2
3	F	30	21	0.7	134	4.8	683.4

SUPPLEMENTAL MATERIALS AND METHODS

Dosimetry analysis

The ^{11}C-PABA murine data-based human dosimetry was obtained from 4 animals injected with ^{11}C-PABA intravenously and imaged over 85 minutes. The PET images were first co-registered to the CT images. Partial regions of interest were drawn on the CT images of a selection of mouse organs: brain, heart, lungs, liver, muscle, large intestine, and bone marrow to obtain the activity concentration in 17 measured time-points after injection (0, 5, 10, 15, 20, 25, 30, 35, 40, 45, 50, 55, 60, 65, 70, 75, 80 and 85 min). Whole-organ contours were drawn to measure the activity in the kidneys and bladder of the mice. The activity concentration (mean value) in Bq/ml and activity (Bq) was recorded for each mouse. The measured activity values were decay corrected to the time of the start of the acquisition (T0).

To account for physical decay of ^{11}C as needed for dosimetry calculations, effective activity concentration values were obtained using the following expression:

$$Act.Conc.(eff.) = Act.Conc.(biol.)\ x\ Exp(-\lambda(C\_11) * t)$$

where $\lambda(C\_11) = \ln(2)/t_{1/2}$ is the physical lambda of ^{11}C and $t_{1/2} = 20.33$ h for ^{11}C, t is the time

The effective activity concentration values were divided by the injected activities in each mouse to obtain fraction of injected activity per unit volume (FIA/cc). Average FIA/cc values were calculated from the four mice data, multiplied by the mouse organ volume based on the MOBY mouse model (*19*) and then divided by the mouse organ mass for the 25 g reference mouse model (*19*) to obtain average FIA/g for each organ.

The following equation was used to convert mouse activity data to human:

$$[FIA/organ]_H = [FID/g]_M \cdot OM_H \cdot \frac{TBM_M}{TBM_H}$$

where:

TBM_M	Total body mass of the mouse (set to 19.7 g)
OM_H	Human organ mass (using organ masses from OLINDA EXM)
TBM_H	Human total body mass (set to 73.7 kg, from OLINDA EXM compilation of organ masses)

The total heart mass (tissue plus blood in chambers, 620 g for female and 840 g for male) was used when converting mouse heart time-activity to human heart time-activity data. The human bladder time-activity data were obtained using both human bladder tissue only mass (bladder-wall, 35.90 g for female and 47.60 g for male), and, bladder + contents mass (bladder contents, 200 g for both male and female) (*20*).

The activity in the remainder of the body for the mouse was calculated by subtracting the measured whole-body (whole FOV) activity by the sum of the activity data of the measured organs. For each measured time-point in the dynamic PET data the ratio of the body-remainder activity to the whole-body activity was calculated for the average mouse time-activity data. The calculated human organ time-activity data were summed up and multiplied by the ratio of the remainder of body activity to the WB activity derived from the mouse data in order to estimate remainder of body activity in human.

The MIRD Committee S-value methodology (*18*), as implemented in the OLINDA/EXM software package (*17*), was used to perform the absorbed dose calculations. The S-value methodology provides the absorbed dose to a target tissue as the sum of dose contributions from all of the radioactivity-containing (source) tissues. The S-value is usually obtained by Monte-

Carlo simulation that is based upon a standard or reference geometry of the patient and the decay characteristics and emission spectrum of the radionuclide. S-values for a number of source and target tissue combinations and a large number of radionuclides have been previously incorporated in OLINDA/EXM. Once the absorbed dose for a series of organs is obtained, the effective dose may be calculated using tissue weighting factors.

Time-activity graphs were obtained for the following human organs (both male and female) based on the provided murine data: brain, heart, lungs, liver, muscle, large intestine, bladder, kidneys and bone-marrow; fit using a mono-exponential function and integrated from 0 to infinity to obtain the time-integrated activity coefficient (TIAC) or residence time.

Adult female phantom or adult male phantoms were used and absorbed dose calculations were performed for ^{11}C using the calculated TIAC values for the given source organs as input in OLINDA/EXM. The absorbed dose to the urinary bladder was estimated using the Bladder model as implemented in OLINDA/EXM (*17*) with a biological half-life of PABA of 1.6 h and bladder voiding period of 1 h.

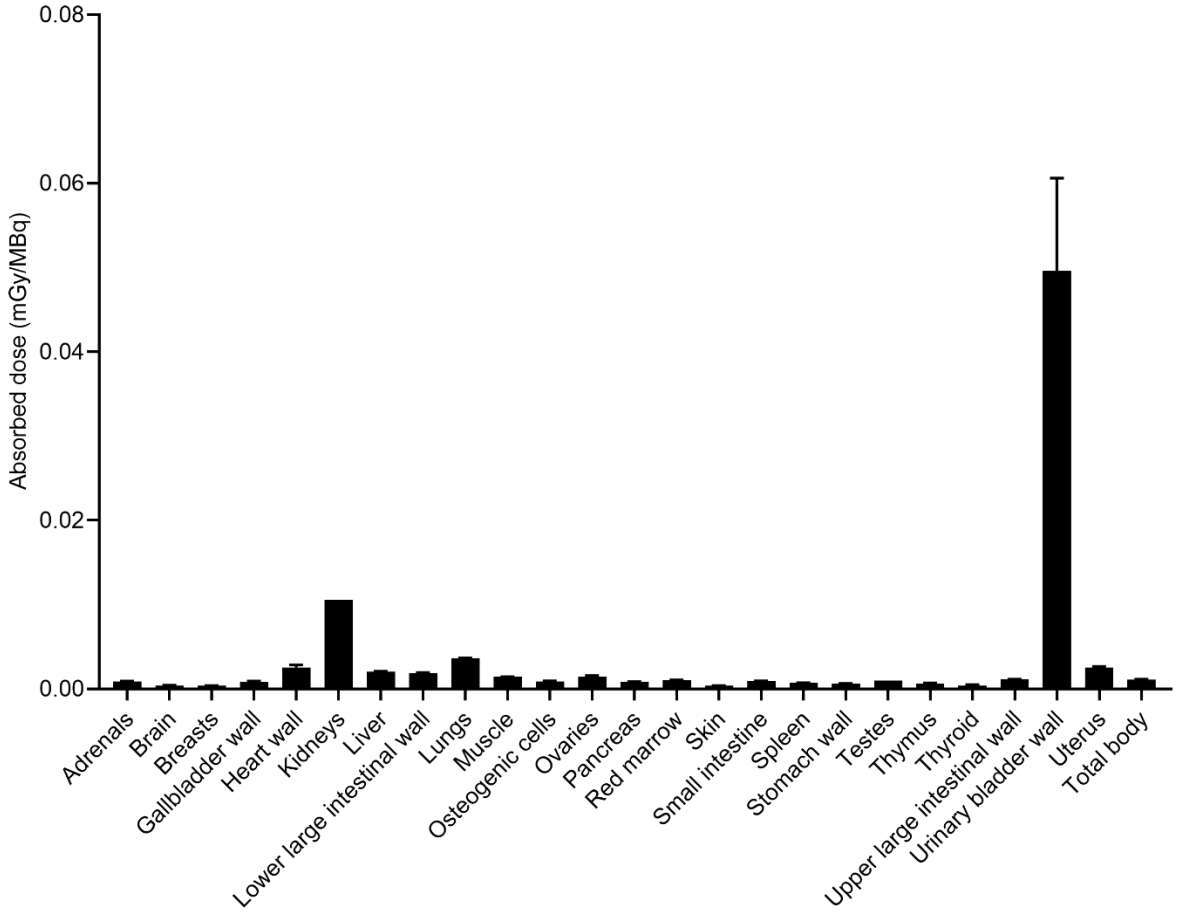

Supplemental Figure 1. Organ-absorbed doses. Data represented as mean ± SD.

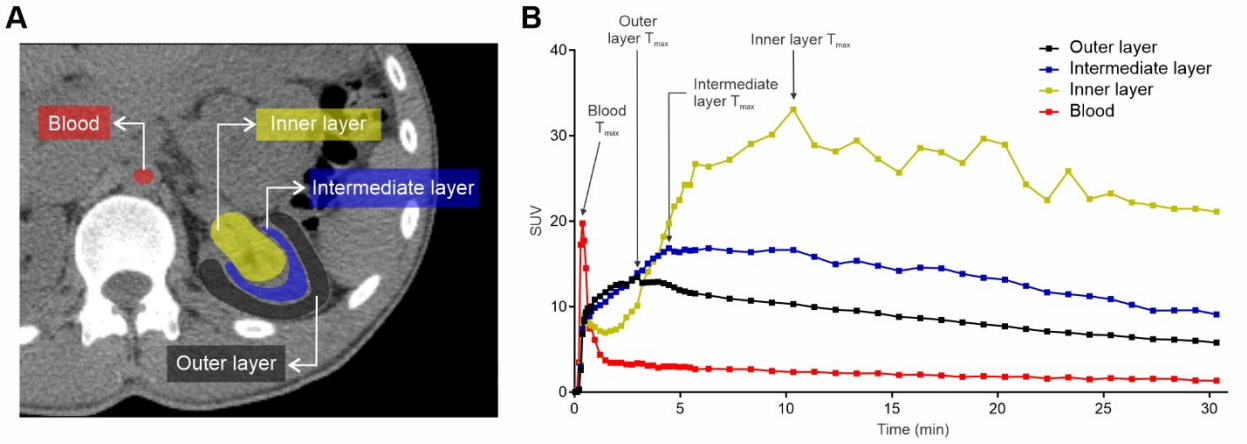

Supplemental Figure 2. Data analysis. (**A**) Representative axial CT slice from a human subject localized over the right kidney shows the representative volumes of interest (VOIs) that were drawn for on five consecutive sections for analysis. (**B**) Time-activity curves for ^{11}C-PABA were derived from the three-dimensional VOIs encompassing the abdominal aorta, renal cortex (outer layer), renal pelvis (inner layer), and the intermediate layer for both right and left kidneys.

Supplemental Table 1. Time-Integrated Activity Coefficients (TIAC). Data represented as mean ± SD.

Site	TIAC (h)
Brain	0.001 ± 0.0002
Heart	0.006 ± 0.0012
Lungs	0.011 ± 0.0018
Liver	0.008 ± 0.0018
Muscle	0.077 ± 0.0265
Large intestine	0.001 ± 0.0001
Bladder wall	0.031 ± 0.0061
Bladder contents	0.146 ± 0.0000
Kidneys	0.011 ± 0.0006
Bone marrow	0.004 ± 0.0004
Remainder of Body	0.014 ± 0.0038

Supplemental Table 2. Absorbed dose estimates. Data represented as mean ± SD.

Site	Estimate (mGy/MBq)
Adrenals	0.0009 ± 0.00002
Brain	0.0004 ± 0.00002
Breasts	0.0004 ± 0.00003
Gallbladder wall	0.0008 ± 0.00008
Heart wall	0.0026 ± 0.00029
Kidneys	0.0106 ± 0.00000
Liver	0.0020 ± 0.00006
Lower large intestinal wall	0.0019 ± 0.00009
Lungs	0.0037 ± 0.00002
Muscle	0.0014 ± 0.00003
Osteogenic cells	0.0009 ± 0.00006
Ovaries	0.0015 ± 0.00011
Pancreas	0.0008 ± 0.00006
Red marrow	0.0011 ± 0.00001
Skin	0.0004 ± 0.00003
Small intestine	0.0009 ± 0.00003
Spleen	0.0007 ± 0.00002
Stomach wall	0.0006 ± 0.00005
Testes	0.0010 ± 0.00001
Thymus	0.0006 ± 0.00008
Thyroid	0.0004 ± 0.00009
Upper large intestinal wall	0.0011 ± 0.00001
Urinary bladder wall	0.0496 ± 0.01103
Uterus	0.0025 ± 0.00014
Total body	0.0011 ± 0.00006

Supplemental Video. ^{11}C-PABA dynamic PET/CT in a human subject. The ^{11}C-PABA signal is observed in a maximum intensity projection video of the dynamic PET of a representative human subject over 30 minutes. Data visualization was performed using Imager 4-D (*21*).